

Computational investigations of optoelectronic and thermoelectric properties of $\text{Cs}_2\text{AuSbX}_6$ (X = Cl, Br, I) double perovskites for energy harvesting devices

S. Maqsood ^{a,b,*}, S. Mumtaz ^c, M. A. Javed ^d, M. Attiqus Salam ^{a,e},
Khalid M. Elhindi ^f

^a Department of Physics, Govt, Graduate college of science, Wahdat road, Lahore-54000

^b Centre for Advanced Studies in Physics (CASP), GC University, Lahore -54000

^c Department of Electrical and Biological Physics, Kwangwoon University, Seoul 01897, South Korea

^d Department of Mathematics, GC University, Lahore -54000, Pakistan

^e Department of physics, GC University, Lahore -54000, Pakistan

^f Plant Production Department, College of Food & Agriculture Sciences, King Saud University, P.O. Box 2460, Riyadh 11451, Saudi Arabia

In this study, we present an empirical investigation into the characteristics of halide double perovskites $\text{Cs}_2\text{AuSbX}_6$ (X = Cl, Br, I) with an emphasis on structural, mechanical, and optoelectronic, along with thermal electricity capabilities. The assessment of thermal and structural durability involves the measurement of the enthalpy of manufacturing & the tolerance ratio. Replacing chlorine (Cl) with bromine (Br) and iodine (I) at the same location in the structure resulted in a surge in the lattice characteristic and a decrease in the bulk elasticity. The calculation of the modulus for elasticity using coefficients of elasticity demonstrated their flexible characteristics. The examination of the electrical band structure revealed that it possesses an indirect band gap characteristic. The applicability of many characteristics, such as the constant of dielectric, extinction coefficients, reflectivity, electronic conductivity, heat conductivity, as well as Seebeck coefficient, is emphasized for photovoltaic and thermal gadgets.

(Received September 29, 2024; Accepted December 5, 2024)

Keywords: Thermal properties, Optical features, Double perovskites halide, Indirect type of band gap semiconductors material

1. Introduction

The exponential growth of the global population and the extensive utilization of various advanced electronic devices have led to a continuous surge in energy requirements that cannot be met by present fossil fuels [1, 2]. In order to address the increasing global energy consumption, it has become crucial to attain renewable and environmentally friendly energy sources [3]. Experts are actively seeking cost-effective, eco-friendly, and very efficient energy alternatives to fulfill the demand [4]. Solar power is the optimal choice among all forms of sustainable energy due to its accessibility and eco-friendliness [5]. Based on the research findings, harnessing a single hour of light from the sun can generate sufficient electrical energy to satisfy the global electricity need for an entire year. Solar energy is an abundant and powerful source of electricity. If we harness and turn it into electrical power, it has the potential to sustain the global population for a duration of twenty-seven years, in the current form [6, 7]. All the energy in petroleum and coal is the same as the amount of solar radiation that the Earth receives in three days continuously [8, 9]. Solar power refers to the electromagnetic radiation emitted by the sun, which can be harnessed to generate either warmth or electricity through the use of solar cells [10]. The solar power cells are available in three different generations. The initial solar cells were durable and dependable, utilizing silicon

* Corresponding author: saba.maq.55@gmail.com
<https://doi.org/10.15251/DJNB.2024.194.1865>

as their basic material, but they were also costly [11]. Silicon-based solar cells undergo a more intricate manufacturing procedure and have a reduced transformation of energy yield. The second-generation thin-film solar cells, however less expensive, have lower efficiency [12]. Perovskite-based solar power cells are a type of third-generation photovoltaic cells that offer a combination of low cost and high performance. However, they are still in the process of development [13]. Perovskite-solar panels have had substantial growth in the past decade, with their efficiency increasing from 3.8% in 2009 to 25% currently [14]. The family of perovskite sunlight harvesting cells that is most extensively researched is the hybrid organic-inorganic perovskite bearing lead with halide APbX_3 [15]. The remarkable ability of Pb halide-based perovskites to efficiently transform sunlight into electrical power has captured the interest of scientists. Perovskites made based on lead (Pb) exhibit higher efficiency and possess a stable framework, but they are also known for their hazardous properties [16]. Because of considerations over the welfare of humans and surroundings, the toxic properties of Pb (lead) restrict its usage in various industrial processes [17]. Thus, efforts have been made to replace the poisonous Pb with harmless Sn^{+2} and Ge^{+2} ions. These positively charged ions are susceptible to oxidation, which in turn decreases the durability of cell structure [18]. Substituting Pb with non-toxic elements by hetero valent metal substitutions is a promising method.

Halide double-perovskites have emerged as a possible alternative for exploring Pb-free formulations in optical devices. Typically, these compounds are denoted as $\text{A}_2\text{B}'\text{B}''\text{X}_6$, with A typically belonging to the alkali community, B' and B'' being transition elements, together with X standing for the halide ionic group (Chlorine, Bromine, Iodine). These compounds are quite adaptable in terms of their architecture, allowing them to be used in a wide range of applications, such as photovoltaics, photocatalysis, optoelectronics, and thermoelectrics [19]. This process involves the substitution for both divalent Pb^{2+} ions with a combination of a trivalent compound B^{3+} ion together with a monovalent B^+ ion. As a result, $\text{A}_2\text{B}'\text{B}''\text{X}_6$ double-perovskites are formed, which maintain the 3-dimensional crystalline composition with charge neutrality of perovskite [20]. Due to the not hazardous features of DPs, scientists are actively researching Pb-free DPs solar powered cells that demonstrate outstanding reliability & efficiency. Halide-based double perovskites are highly attractive because of their lack of toxic Pb^{2+} ions and their exceptional mechanical and thermal endurance, as well as their ability to tune the band edges [21]. The utilization of metal-based halide-perovskites, namely organic and inorganic hybrid compounds, in solar power cells has significantly increased the significance of PV studies in the past decade [22]. A multitude of professionals are presently engaged in the development of renewable energy sources on a global scale, with a substantial proportion of this cohort directing their efforts towards solar cells composed of perovskite. However, there still remain several obstacles that need to be overcome before solar energy cells made from perovskite can be successfully commercialized. The challenges at hand involve discovering cost-effective and efficient production methods, enhancing moisture resistance to enable outdoor functionality without the need for expensive enclosures, and identifying alternative metal halides that do not contain environmentally harmful substances such as lead [23]. Thus, there remains ample potential for further exploration in order to assess the appropriateness of HDPs for applications in optics. Based on an extensive review of the scientific literature, it has been discovered that there is a lack of theoretical research on the photonic characteristics of $\text{Cs}_2\text{AuSbX}_6$ where, Cl, Bromine, and I are the components of X. For that reason, the primary objective of this research is to examine $\text{Cs}_2\text{AuSbX}_6$ double perovskites previously unexplored. The element potassium is present in nature in its elemental form with the ability to greatly decrease the cost of manufacturing devices [24]. Consequently, we examined Cs, the fundamental, mechanical in nature, optoelectronic, & thermoelectric characteristics using the first principle method. We are confident that this comprehensive research of the attributes of the compounds will facilitate the development of new materials with specific required characteristics. This research will undoubtedly contribute valuable insights to the current understanding of double perovskite, providing aspiring researchers with new avenues for exploring those substances for innovative usage.

1.1. Computational analysis

The DFT was employed to study the various physical responses exhibited by Double Perovskites $\text{Cs}_2\text{AuSbX}_6$ as part of the WIEN2k coding system. The optimization of the structure was carried out utilizing the PBEsol-GGA method [26]. As part of the optimization procedure, a k-mesh measuring $10 \times 10 \times 10$ was built. From this mesh, the algorithm autonomously chose 47 points. Furthermore, the parameters $R_{\text{MT}} \times K_{\text{max}}$ or G_{max} had been given values of 8 and 16, respectively. Here, R_{MT} refers to the radius for the muffin tin atom, in order while K_{max} indicates the highest possible value for the K-vector. The power convergence requirements were established at a threshold of 10^{-5} Ry. In addition, the modified Becke and Johnson potential (mBJ) has been employed to accurately calculate the electrical bandwidth gaps of the tested DPs [27]. Subsequently, the BoltzTrap algorithm, which is centered on the Boltzmann-transport concept, was utilized to evaluate the thermoelectric properties of HDPs $\text{Cs}_2\text{AuSbX}_6$ ($X = \text{Cl, Br, I}$). [28].

2. Results and discussion

2.1. Analysing the crystal composition

Figure 1 shows the internal layout of the functional cells, which includes $\text{Cs}_2\text{AuSbX}_6$ ($X = \text{Cl, Br, I}$). The dimension of the cell is face-centered cubic (FCC) and belongs to the Fm-3m spatial group. Given a crystallography perspective, Cs elements occupy interstitial positions having fractional dimensions of (0.25, 0.25, 0.25), whereas Au, Sb, and X have fractional locations of (0, 0, 0), (0.5, 0.5, 0.5), along with (x, 0, 0) correspondingly [29]. The cesium atoms exhibit an atomic coordination number of 12, while the Sb/Au atoms have a coordinating number of 6, as they are surrounded by 12 & 6 halide ions, respectively. The individual atoms of potassium (Cs) and scandium (Sb) are depicted as purple and blue balls, respectively, in Fig.1. The elements of gold (Au) with X-atoms are symbolized by red and green spheres, respectively. The ground-state configuration of the unit cell has been optimized using its lattice parameter (a_o) and bulk moduli (B_o) (refer to Table 1). It was noted how a_o 's setting by default is $\text{Cs}_2\text{AuSbCl}_6$ equals 10.75\AA , which raised to 11.27\AA for $\text{Cs}_2\text{AuSbBr}_6$ and 12.01\AA for $\text{Cs}_2\text{AuSbI}_6$. Additionally, the computed values for a_o were similar to previous theoretical estimates [30]. The rise in the value of a_o (\AA) is attributed to the larger radius of the ion of the halogens. The graphs illustrating the optimization of the energy volume can be seen in Figure 2. As the dimension of X increased, B_o gradually diminished due to its inverse relationship with a_o . The bulk modulus (B_o) of $\text{Cs}_2\text{AuSbCl}_6$ is 31.01GPa , and it reduced down 26.27GPa by $\text{Cs}_2\text{AuSbBr}_6$ and 21.68GPa for $\text{Cs}_2\text{AuSbI}_6$ [31]. To assess the thermodynamic properties and structural strength of a material, one can calculate the value of the tolerance factor " t_f " as well as the enthalpy of formation (ΔH_f) by applying the equations provided [32, 33].

$$t_f = (r_{\text{Cs}} + r_{\text{Cl/Br}}) / \sqrt{2} (r_{\text{B}} + r_{\text{Cl/Br}}) \quad (1)$$

The atomic radius of L & Cl/Br elements are represented by r_{Cs} and $r_{\text{Cl/Br}}$, respectively, while r_{B} denotes the mean atomic radii for Sb and Au elements. The structural durability of the perovskite compounds was assessed by examining the amount of t_f , which is determined by the respective ionic radius from the three types of ions involved. For a stable structure, the number of t_f must fall within the range of 0.81 to 1.11 [34]. The computed values of t_f for $\text{Cs}_2\text{AuSbX}_6$ ($X = \text{Cl, Br, I}$) were 0.94, 0.92, and 0.91, respectively, which confirmed the stable structure of these compounds.

$$\Delta H_f = E_{\text{Total}}(K_a S_c b A_u c \text{Cl/Br}_d) - a E_{\text{Cs}} - b E_{\text{Au}} - c E_{\text{Sb}} - d E_{\text{Cl/Br}} \quad (2)$$

The program computes the difference between the energy (formation energy) among the compounds $\text{Cs}_2\text{AuSbX}_6$ ($X = \text{Cl, Br, I}$) as well as the bulk unit cells of Cs, Au, Sb, and Cl/Br elements. The symbols E_{Cs} , E_{Sb} , E_{Au} , and $E_{\text{Cl/Br}}$ represent the energy levels of cesium (Cs), Antimony (Sb), gold (Au), and chlorine/bromine (Cl/Br) Elements, respectively. The recorded

values for the change in enthalpy (ΔH_f) of $\text{Cs}_2\text{AuSbCl}_6$, $\text{Cs}_2\text{AuSbBr}_6$, and $\text{Cs}_2\text{AuSbI}_6$ had been -2.31 eV, -2.03 eV, and -1.89, respectively. Due to the unfavorable concentrations of ΔH_f , every single one of these compounds is stable.

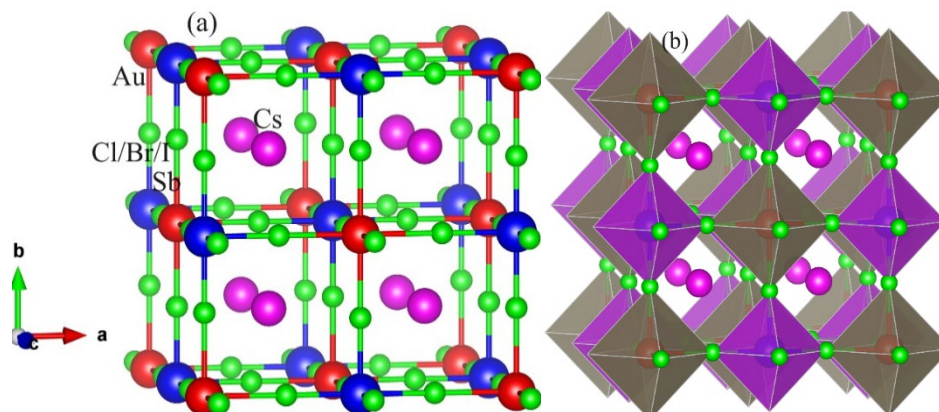


Fig. 1. Crystal structure plot of HDPs $\text{Cs}_2\text{AuSbX}_6$ ($X = \text{Cl}, \text{Br}, \text{I}$) in (a) ball format and (b) polyhedral format.

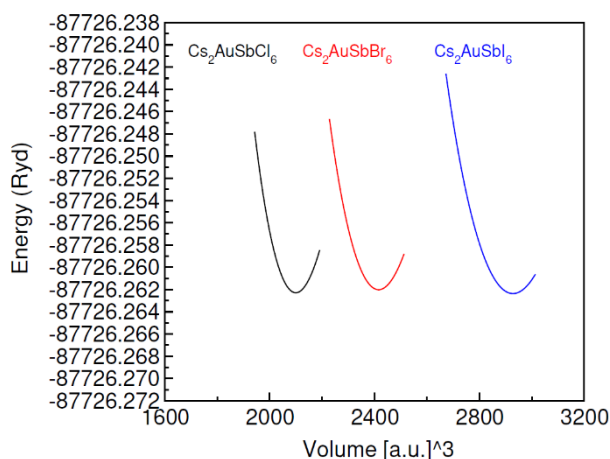


Fig. 2. Energy versus volume plot of investigated HDPs $\text{Cs}_2\text{AuSbX}_6$ ($X = \text{Cl}, \text{Br}, \text{I}$).

2.2. Mechanical properties

The solution of a set of non-linear problems symbolized by a tensor matrices is necessary for the analysis of the materials' mechanical behavior. This process determines various modulus values. For cubic substances, the physical reaction of the constituent substance can be defined by three variables: C_{11} , C_{12} , and C_{44} [35]. The stability standards by "Born" evaluate and rank cubic compounds based on their elastic coefficients [36]. The substitution of chlorine (Cl) with bromine (Br) and iodine (I) resulted in a decrease in the elastic constants along with the moduli of elasticity. This suggests that the materials now require fewer stresses to undergo plastic distortion. Before utilizing whatever substance for a certain purpose, it is essential to determine its mechanical attributes, namely whether it is rigid or flexible. The decision is made by evaluating the estimated amounts of the Poisson (ν) with Pugh (B/G) ratios. Ductile materials have an index of B/G greater than 1.75 plus a value of ν greater than 0.26, conversely, they are brittle [37]. Furthermore, B/G values for $\text{Cs}_2\text{AuSbCl}_6$, $\text{Cs}_2\text{AuSbBr}_6$, and $\text{Cs}_2\text{AuSbI}_6$ were 2.31, 2.11 and 2.08 separately. The values of ν for these substances were 0.31, 0.30, and 0.29. These results indicate that all three materials $\text{Cs}_2\text{AuSbCl}_6$, $\text{Cs}_2\text{AuSbBr}_6$, and $\text{Cs}_2\text{AuSbI}_6$ possess malleability.

Table 1. Calculated values of lattice constant $a_0(\text{\AA})$, bulk modulus $B_0(\text{GPa})$, enthalpy of formation (ΔH_f), and elastic parameters of hybrid double Ps $\text{Cs}_2\text{AuSbX}_6$ ($X = \text{Cl}, \text{Br}, \text{I}$).

| Parameters | $\text{Cs}_2\text{AuSbCl}_6$ | $\text{Cs}_2\text{AuSbBr}_6$ | $\text{Cs}_2\text{AuSbI}_6$ |
|-------------------|------------------------------|------------------------------|-----------------------------|
| | PBEsol-GGA | PBEsol-GGA | PBEsol-GGA |
| $a_0(\text{\AA})$ | 10.75 | 11.27 | 12.01 |
| B_0 (GPa) | 31.01 | 26.27 | 21.68 |
| ΔH_f (eV) | -2.31 | -2.03 | -1.89 |
| t_f | 0.94 | 0.92 | 0.91 |
| C_{11} | 48.50 | 43.96 | 37.04 |
| C_{12} | 22.04 | 17.64 | 14.04 |
| C_{44} | 13.45 | 12.05 | 9.75 |
| B | 30.86 | 26.41 | 21.70 |
| G | 13.36 | 12.48 | 10.41 |
| Y | 35.02 | 32.35 | 26.93 |
| B/G | 2.31 | 2.11 | 2.08 |
| ν | 0.31 | 0.30 | 0.29 |
| A | 0.94 | 0.91 | 0.85 |

Ref. [30]^a

Table 2. Maximum and minimum value and elastic anisotropy for $\text{Cs}_2\text{AuSbX}_6$ ($X = \text{Cl}, \text{Br}, \text{I}$).

| Compounds | Young's Modulus (Y) (GPa) | | | Linear compressibility (β)(TPa^{-1}) | | | Shear modulus (G) (GPa) | | | Poisson's ratio (ν) | | |
|------------------------------|---------------------------|--------------|-----------|---------------------------------------------------------|----------------|------------|-------------------------|--------------|-----------|---------------------------|--------------|------------|
| | Y_{\min} | Y_{\max} | A | β_{\min} | β_{\max} | A | G_{\min} | G_{\max} | A | ν_{\min} | ν_{\max} | A |
| $\text{Cs}_2\text{AuSbCl}_6$ | 0.02061 9 | 0.02829 4 | 1.37 2 | 92580 | 92580 | 1.000 0 | 0.01889 6 | 0.07434 9 | 3.93 5 | -0.8375 | - 0.45443 | 0.542 6 |
| $\text{Cs}_2\text{AuSbBr}_6$ | 0.02274 8 | 0.03286 2 | 1.44 5 | 79240 | 79240 | 1.000 0 | 0.01899 7 | 0.08298 8 | 4.36 8 | - 0.83527 | - 0.40127 | 0.480 4 |
| $\text{Cs}_2\text{AuSbI}_6$ | 0.02699 8 | 0.04006 9 | 1.48 4 | 65120 | 65120 | 1.000 0 | 0.02173 9 | 0.10256 8 | 4.71 8 | - 0.84066 | - 0.37905 | 0.450 9 |

2.3. Elastic anisotropy

Material isotropy plays a major role in predicting micro-hardness and the research of mechanical strength. High degrees of possible outcome of elastic-anisotropy is the emergence of microcracks in some materials. A cubic structure does not always have isotropic elastic characteristics. The degree of a solid's elastic anisotropy can be measured using an index known as the Zener anisotropic factor (A). $A=1$ denotes the isotropy of a material; the elastic anisotropies are determined by the percentage variation from unity. For the selected materials, the orientation-dependent 2D and 3D moduli of elastic have designated maximum and minimum values that are listed in Table 2, and the moduli are shown in Fig. 3. This study suggests that materials have use in foldable optoelectronics and device engineering. All compounds exhibit anisotropy as determined by Poisson's ratio (ν), shear modulus (G), linear compressibility (β), and Young's modulus (Y). $\text{Cs}_2\text{AuSbCl}_6$ to $\text{Cs}_2\text{AuSbI}_6$ exhibits an increase in elastic moduli anisotropy. These materials are suitable for applicable in elastic optoelectronic devices because of their anisotropy, mechanical strength, and elastic characteristics.

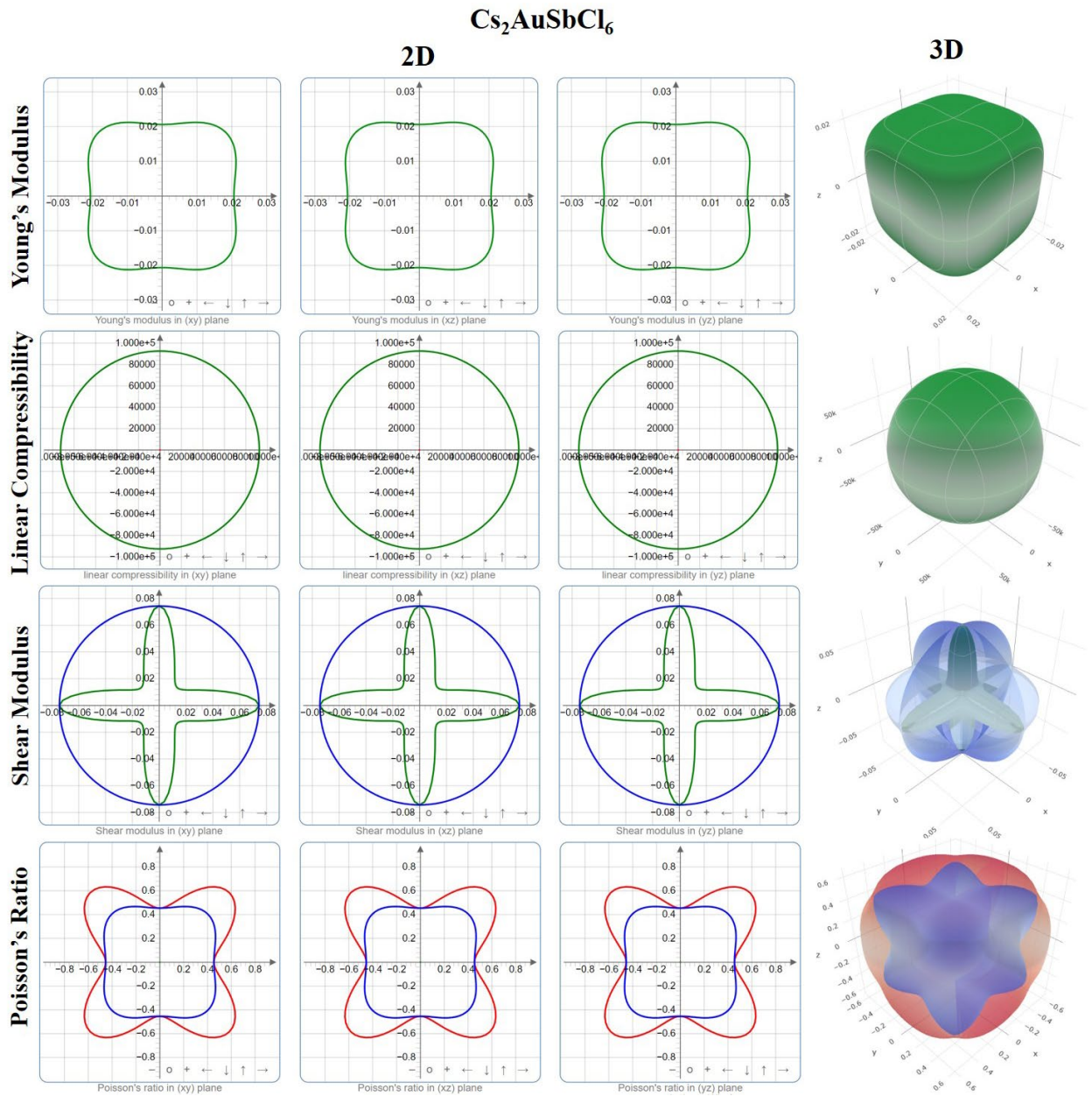


Fig. 3 (a). 2D and 3D elastic moduli depend on the direction for $\text{Cs}_2\text{AuSbCl}_6$.

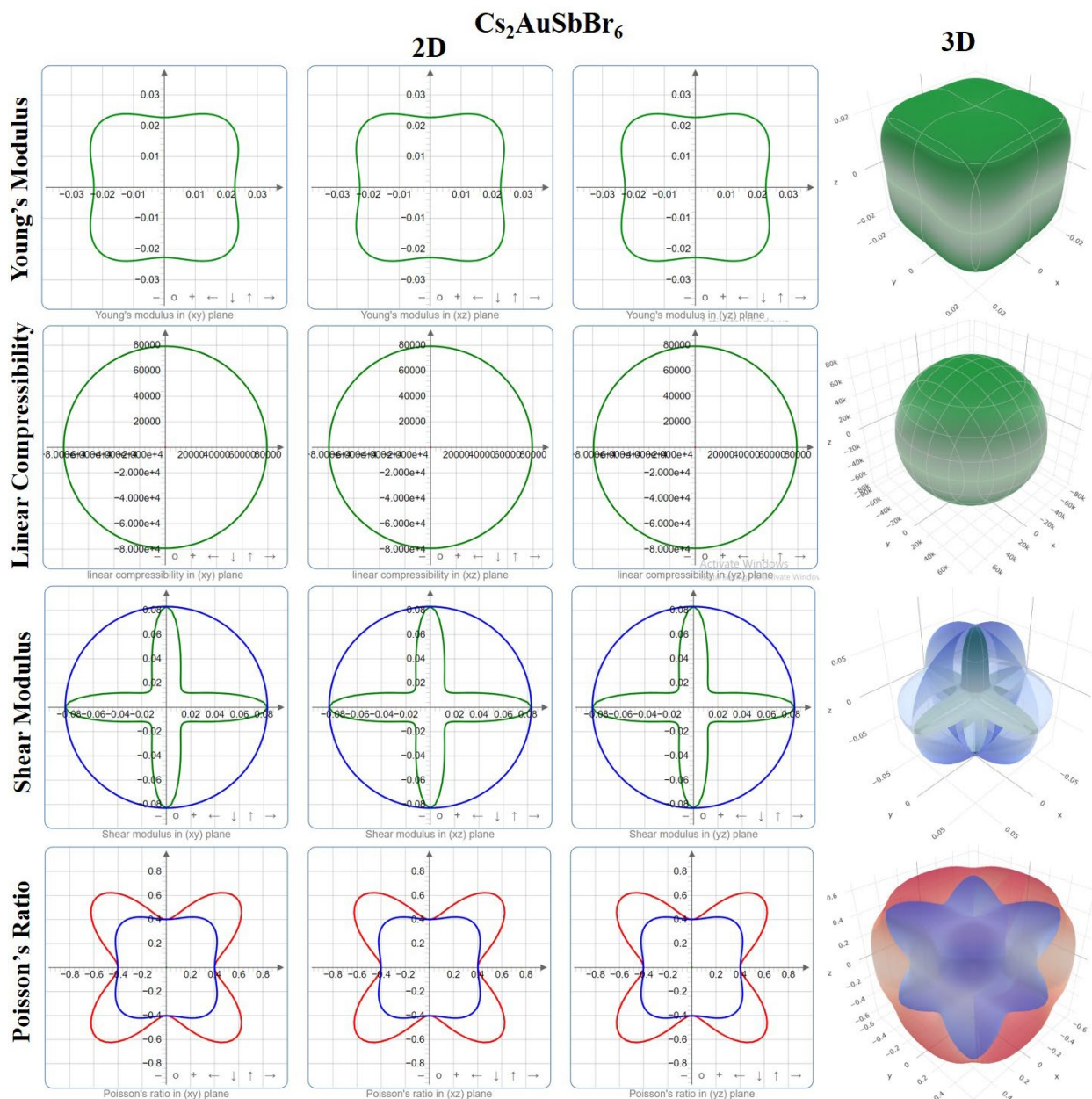


Fig. 3 (b). 2D and 3D elastic moduli depend on the direction for $\text{Cs}_2\text{AuSbBr}_6$

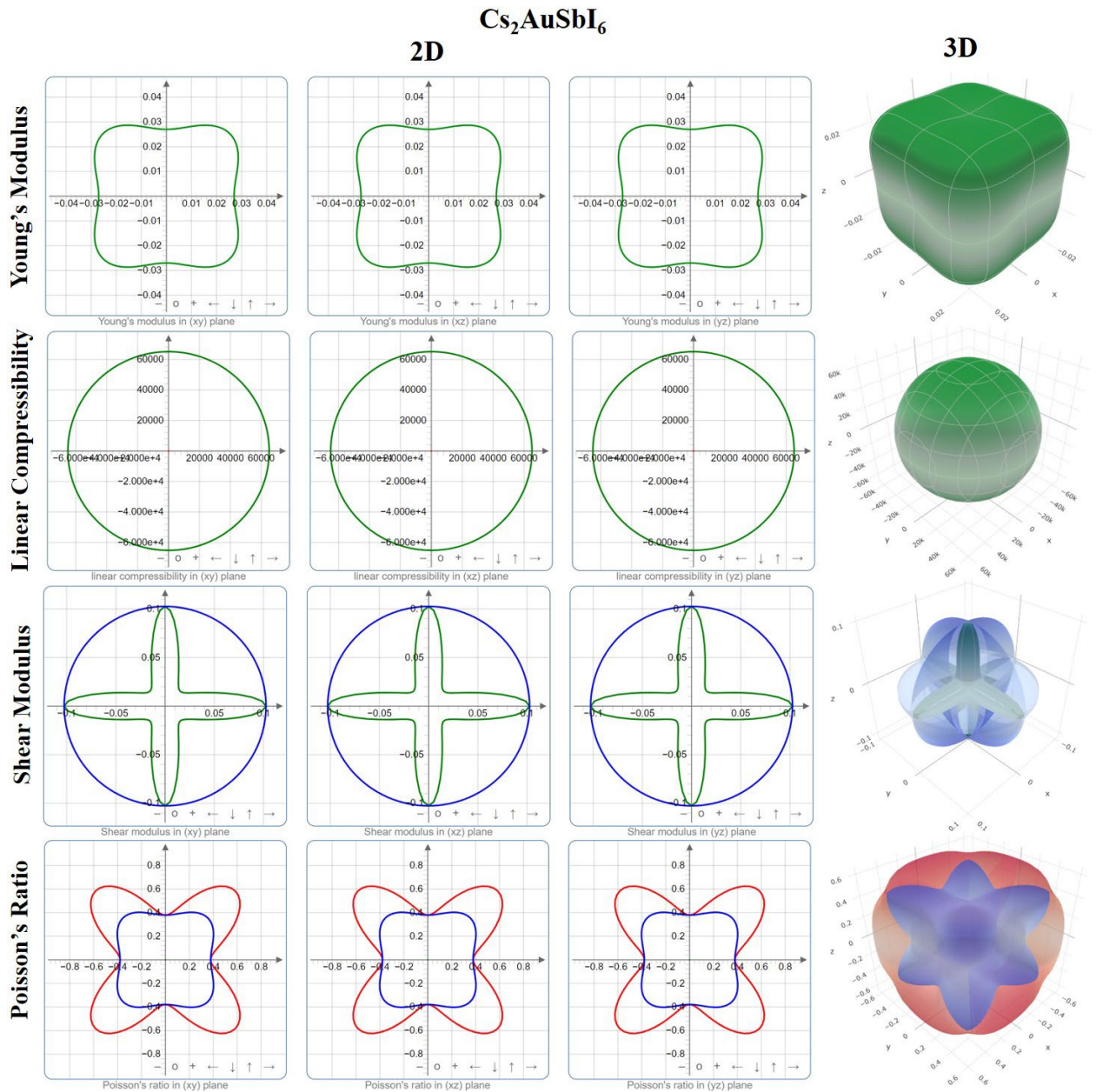


Fig. 3 (c). 2D and 3D elastic moduli depend on the direction for $\text{Cs}_2\text{AuSbI}_6$.

2.4. Density of states and band structure

The arrangement of electronic bands is crucial in determining the practical applications of any compound [38]. The study found that the valence band maximum and the conduction band minimum for all three combinations occur at the L and X symmetric points [39]. Due to the fact that the band's boundaries lie at well defined symmetry positions, it is evident that the material has a bandgap that is indirect and exhibits semiconducting properties, Figure 4. A more comprehensive understanding of the variations in bandgap frequency can be achieved by analyzing the density of the state's (DOS) plot, as depicted in Figure 5. The DOS governs the number of energy states that are accessible within a given range of energy. Density of States plots show the levels of atomic energy that contribute to the nearest band boundaries. Elements' electronegativity along with atomic number largely dictate where these states lie inside the band. [40, 41]. Figure 5 displays the DOS graphs. This data reveals that the 5d states of Au have a crucial impact on the highest energy levels in the valence band, whereas the 4p contents of Sb considerably participate in the creation

of the lowest energy levels in the conduction spectrum. The modulation of bands with a halogen replacement can be comprehended by analyzing the Partial Density of States (PDOS).

Table 3. Calculated bandgap (E_g (eV) with mBJ potential and optical parameters at 0 energy of Cs_2AuSbX_6 ($X = Cl, Br, I$) halides.

| Parameters | $Cs_2AuSbCl_6$ | $Cs_2AuSbBr_6$ | Cs_2AuSbI_6 |
|-----------------|----------------|----------------|---------------|
| | mBJ | mBJ | mBJ |
| E_g (eV) | 1.36 | 0.81 | 0.27 |
| $\epsilon_1(0)$ | 4.35 | 4.99 | 7.41 |
| $n(0)$ | 1.91 | 2.22 | 2.67 |
| $R(0)$ | 0.1 | 0.18 | 0.21 |

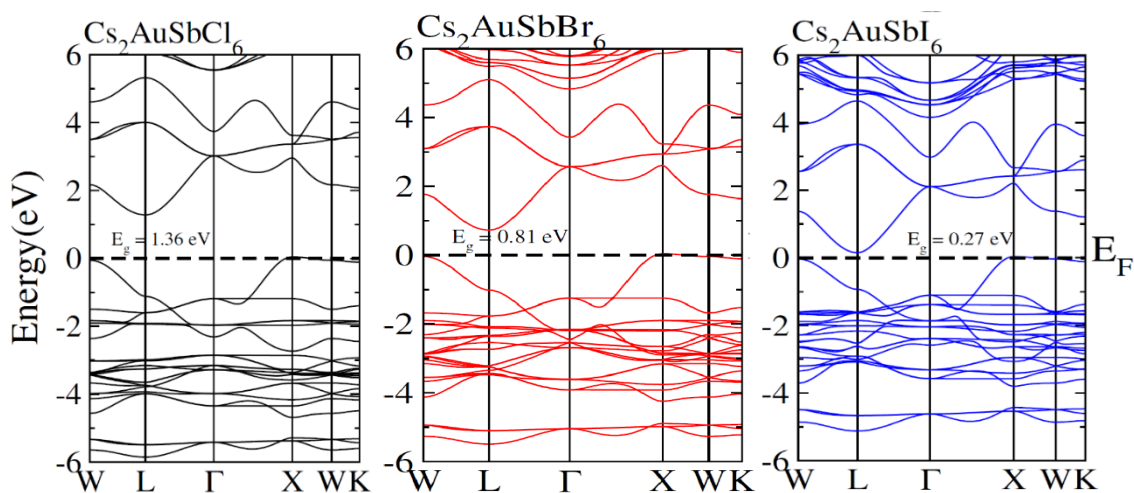


Fig. 4. Calculated electronic band structure for HDPs Cs_2AuSbX_6 ($X = Cl, Br, I$).

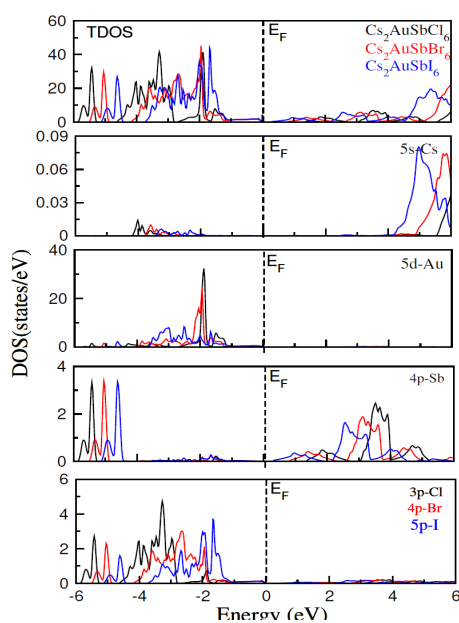


Fig. 5. Calculated total density of stated (DOS) along with partial DOS HDPs Cs_2AuSbX_6 ($X = Cl, Br, I$).

2.5. Optical properties

Electrons are charged particles in an element are stimulated when an external light stream with an energy equal to or greater than its bandgap impacts with the material's outer layer. The stimulated electrons then move across the valence band of a material to the conduction band (CB) [42]. The subsequent recombination among these electrons is influenced by the relative speeds of changeover and replication, which are crucial elements determining the optical characteristics of the solids. Optoelectronic semiconductors have the ability to convert electromagnetic radiation into electrical energy, making them useful in a wide range of applications to meet the energy demands of the increasing population[43]. The figures displayed in Figure 6 illustrate the optical properties of HDPs $\text{Cs}_2\text{AuSbX}_6$ ($X = \text{Cl}, \text{Br}, \text{I}$), specifically the real (ϵ_1) and imaginary (ϵ_2) components of the dielectric constant, in addition to the extinction coefficient (k) absorption coefficient $\alpha(\omega)$, along with refractive index (n) and reflectivity $R(\omega)$ plotted against the energy value of incident photons ranging from 0 to 10 eV [44]. The words ϵ_1 and ϵ_2 represent the phenomena of polarization and the light absorption, respectively. When the energy is a value of zero the static dielectric constant $\epsilon(0)$ shows a rising tendency as the amount of photon energy increases.

The recorded data for the analyzed data points (DPs) are displayed in Table 3, below. The significance level of $\epsilon_1(0)$ for $\text{Cs}_2\text{AuSbCl}_6$ was 4.35, while for $\text{Cs}_2\text{AuSbBr}_6$ it measured 4.99 and for $\text{Cs}_2\text{AuSbI}_6$ it had a value of 7.41. The more significant value of $\epsilon_1(0)$ is believed that the higher polarization observed in DPs comprising I atomic particles, in comparison to Cl as well as Br, is due to their bigger ionic radius. The bandgap energies E_g & $\epsilon_1(0)$ possess an inverse relationship pursuant by the ‘‘Penn’s model formula’’ $\{ \epsilon_1(0) \approx 1 + (\hbar\omega_p/E_g)^2 \}$ [45]. The reason for the difference in the $\epsilon_1(0)$ value between $\text{Cs}_2\text{AuSbCl}_6$, $\text{Cs}_2\text{AuSbBr}_6$, and $\text{Cs}_2\text{AuSbI}_6$ is that the former has an energy band gap of 1.36 eV, whereas the latter has the value equal 0.81 eV and 0.27eV respectively. The peaks shown on the chart are referred to as relaxing peaks [46]. As the atomic radius of the halogens increases, the peaks shift towards smaller frequencies. The exact location of the peaks can be utilized to figure out the relaxation frequency for the compositions. The total mass of the substance and its relaxation frequency have an opposite relationship [47].

The quantity ϵ_1 is defined as the difference between the squares of ‘‘ n ’’ & ‘‘ k ’’, i.e., ($\epsilon_1 = n^2 - k^2$). The value of n can be calculated by taking the cubic root of ϵ_1 , according to Table 3, the calculated $n(0)$ values for $\text{Cs}_2\text{AuSbCl}_6$, $\text{Cs}_2\text{AuSbBr}_6$, & $\text{Cs}_2\text{AuSbI}_6$ were reported as 1.91, 2.22, and 2.67, respectively. It has a reaction that is nearly identical to that of ϵ_1 . Conversely, k exhibits a comparable reaction to that shown by ϵ_2 . The term ϵ_2 provides information regarding the quantity of light captured by the substance [48]. The energy that is absorbed by a photon is measured using its absorption factor (α), which is related to the extinction factor through the equation ($\alpha = 4\pi k/\lambda$) [49]. Figure 6(e) shows the change in α , which indicates the absorption started at 1eV and increased gradually until it reached 10eV. The compound containing I exhibited greater absorption due to the greater amount of electrons accessible for absorbance in comparison with the composition containing Cl as well as Br. The presence of a large number of peaks inside the 1-10 eV zone is indicative of the existence of numerous potential transitions from occupied to unoccupied states. The absorbance spectrum can also be utilized for determining the bandgap value, and this typically exceeds the values calculated from the band layout. The difference between these numbers is credited to the constraints that were used in the Kramer-Kronig formula as well as the range of exchanging potential that was applied in ‘‘Density Functional Theory (DFT)’’[50].

Based upon the reflectivity $R(\omega)$ for the subject matter, the assessment of the quantity that constitutes surface reflections is performed, which has been computed and illustrated in Figure 6(f). The numerical value of R correlated positively with the size given by the halogen, potentially because of the greater quantity of valence electrons accessible for reflection. The significance of such compounds for electronic gadgets is underscored by a minimal value of $R(\omega)$ in the low-power range.

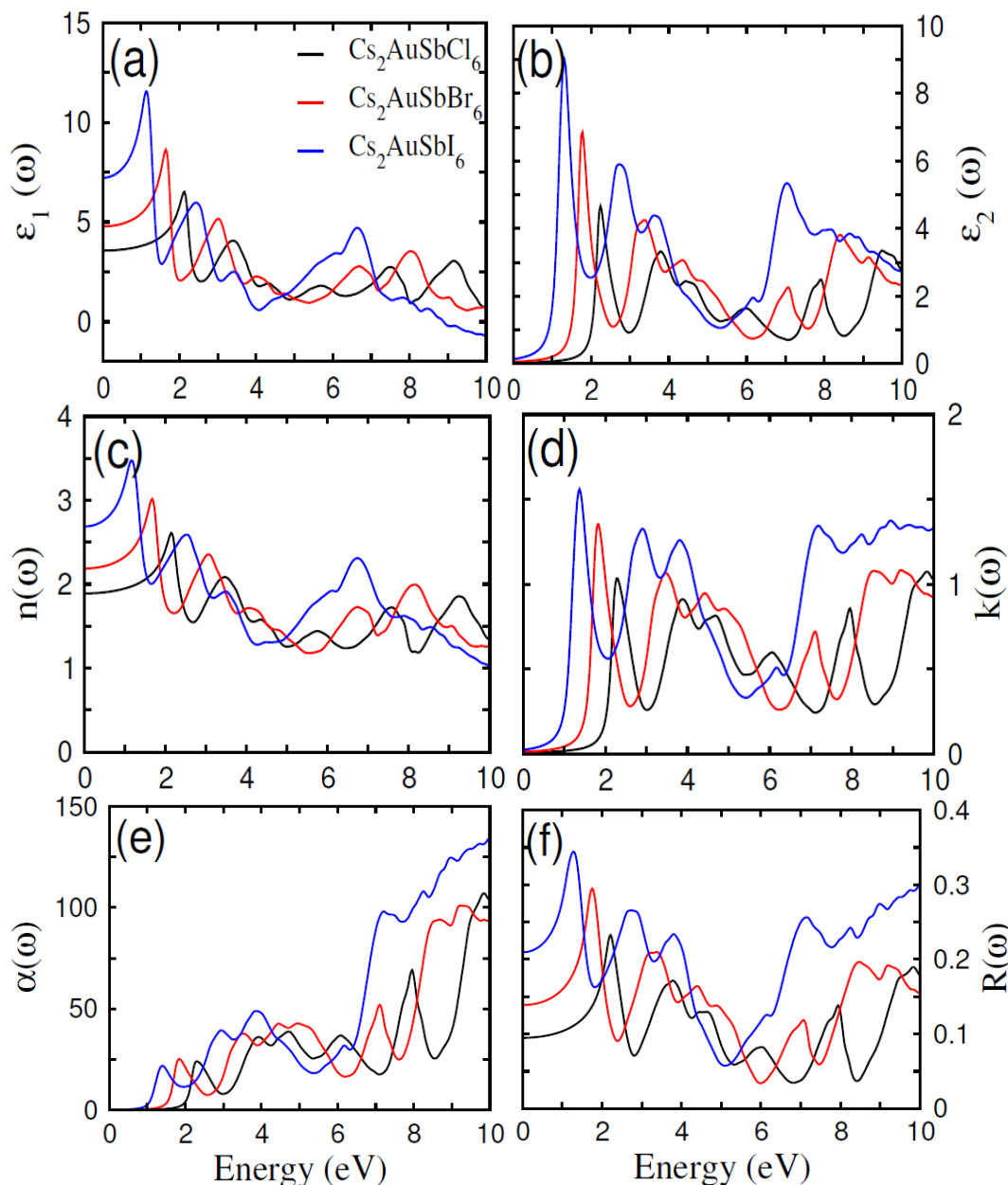


Fig. 6. The calculated (a) real part $\epsilon_1(\omega)$, (b) imaginary part $\epsilon_2(\omega)$, (c) refractive index $n(\omega)$, (d) the extinction co-efficient $k(\omega)$, (e) absorption $\alpha(\omega)$ (10^5 cm^{-1}), (f) reflectivity $R(\omega)$ of HDPs $\text{Cs}_2\text{AuSbX}_6$ ($X = \text{Cl}, \text{Br}, \text{I}$).

2.6. Thermoelectric properties

The thermoelectric characteristics of compounds are determined by two important factors: a power factor ($P = \sigma S^2/\tau$) as well as the figure of merit ($ZT = \sigma S^2/\kappa T$). These factors are dependent upon both electrical (σ/τ) and heat (κ/τ) conductivities, as well as the Seebeck coefficient (S) [51]. To improve the thermoelectric properties of materials, it is necessary for the ratio of electrical conductivity to relaxation time (σ/τ) and the Seebeck coefficient (S) to be great, while the ratio of thermal conductivity to relaxation time (κ/τ) must be modest. The symbol τ indicates a relaxation permanent of time that has a value that is constant, 10^{-14} s [52]. Due to the utilization of the contacting relaxation time approximated values, the readings of conductivity can be divided by the relaxation time. The graph in Figure 7(a) illustrates the relationship between σ/τ and T (K) within the operating temperature range of 300-800 K. It is observed that the corresponding value of σ/τ for (Cl/Br/I) based combinations was $(0.75/0.77/0.79) \times 10^{19} (\Omega \cdot \text{m} \cdot \text{s})^{-1}$ at

300K. As the temperature grew, these values also increased and reached approximately 1.54×10^{19} $(\Omega \cdot m \cdot s)^{-1}$ aimed at each of the compound at temperature 800K. The rise in the ratio “ σ/τ ” signifies when there is an increase in the amount of recipients that are available for transmission, the kinetic energy generated by these particles grows with the temperature rise (T).

The Seebeck coefficient quantifies the magnitude of the potential gradient that arises from a temperature differential between the two edges of the material. The distinction between TDOS (Total Density of States) with PDOS (Partial Density of States) has allowed for the identification of the specific contributions of distinct states in the creation of bands. This distinction has also facilitated the determination of the Seebeck coefficient employing the equation [53, 54].

$$S = 8\pi^2 k_B m^* \omega T (3ch^2)^{-1} (\pi/3\rho)^{2/3}$$

In this context, k_B , m^* , with e represent the Boltzmann constant, effectiveness mass, and charge associated with an electron, while h , T & ρ refer to Plank's constant, the absolute temperature, and carrier density accordingly. The observed values of S were 160, 162.5 and 130 $\mu V/K$ at 300K with all three formulations. These values subsequently rose to 181 & 178 $\mu V/K$ for composites based on Cl and Br at 800K. The results closely align with the previously reported S figures for double perovskites, as seen in Figure 7b.

According to [55,56], thermoelectric materials that perform well ought to possess an S value between 200 $\mu V/K$ and 300 $\mu V/K$. This in-race thermoelectric competitor, Bi_2Te_3 , has an S value of 65 mV/K. Nevertheless, the current research attributes the compound's bipolar conduction and broader bandgap to the tiny value of S . At 300K, the value of κ_e/τ was approximately 1×10^{14} (W/mKs), but it climbed to 6.8 & 5.4×10^{14} (W/mKs) with chlorine and bromine founded alignments, correspondingly, whereas for iodine-based compound it reaches upto 6×10^{14} (W/mKs) following the same rising pattern with warmth as σ/τ (Fig. 7c). At a specific temperature (10^{-5}) the proportions of σ/τ as well as κ_e/τ can be used to determine if a material is suitable for thermoelectric uses.

In order to determine the thermoelectric performance of the product, the power factor (PF) is computed by utilizing the expression $\sigma S^2/\tau$. This calculation is performed without taking into account the contribution of κ_e/τ . Figure 7(e) depicts a plot of the PF relative to temp for the components that are the subject of the investigation. At an approximate temperature of 300K, the amount of the PF for each of the compounds was nearly the same, which is to say, 2.1×10^{14} (W/m.K².s). However, when the temperature increases, the PF significantly increases, reaching 4.68×10^{14} (W/m.K².s) for the compositions based on chlorine and bromine, and 3.6×10^{14} (W/m.K².s) for I-based HDPs [57]. The figure of merit is the last aspect that is utilized in the process of determining the thermoelectric performance of a material by integrating the κ_e/τ component. Figure 7(f) depicts a linear relationship between the value of ZT and the temperature. At a temperature of 300K, the value of ZT is recorded as 0.6/0.61/0.62 for $Cs_2AuSbCl_6$, $Cs_2AuSbBr_6$, and Cs_2AuSbI_6 correspondingly. This value rose with heat (T) and reached 0.65 at 800K for compositions based on chlorine and bromine but decreased near 0.48 for I-based HDPs. The findings that have been reported indicate that the resources that are now being investigated have the potential to be used in thermoelectric devices in the future [58]. As was indicated previously, the Cs_2AuSbX_6 ($X = Cl, Br, I$) complexes that were investigated in this work contain indirect band gaps, which makes them potentially beneficial in the development of novel photovoltaic technologies. This is similar to the situation with silicon. Although these materials are indirect, it is clear from the band gap that they are capable of facilitating improved absorption of a wide variety of solar electromagnetic waves. These contents are therefore deserving of investigation and comprehension because of this.

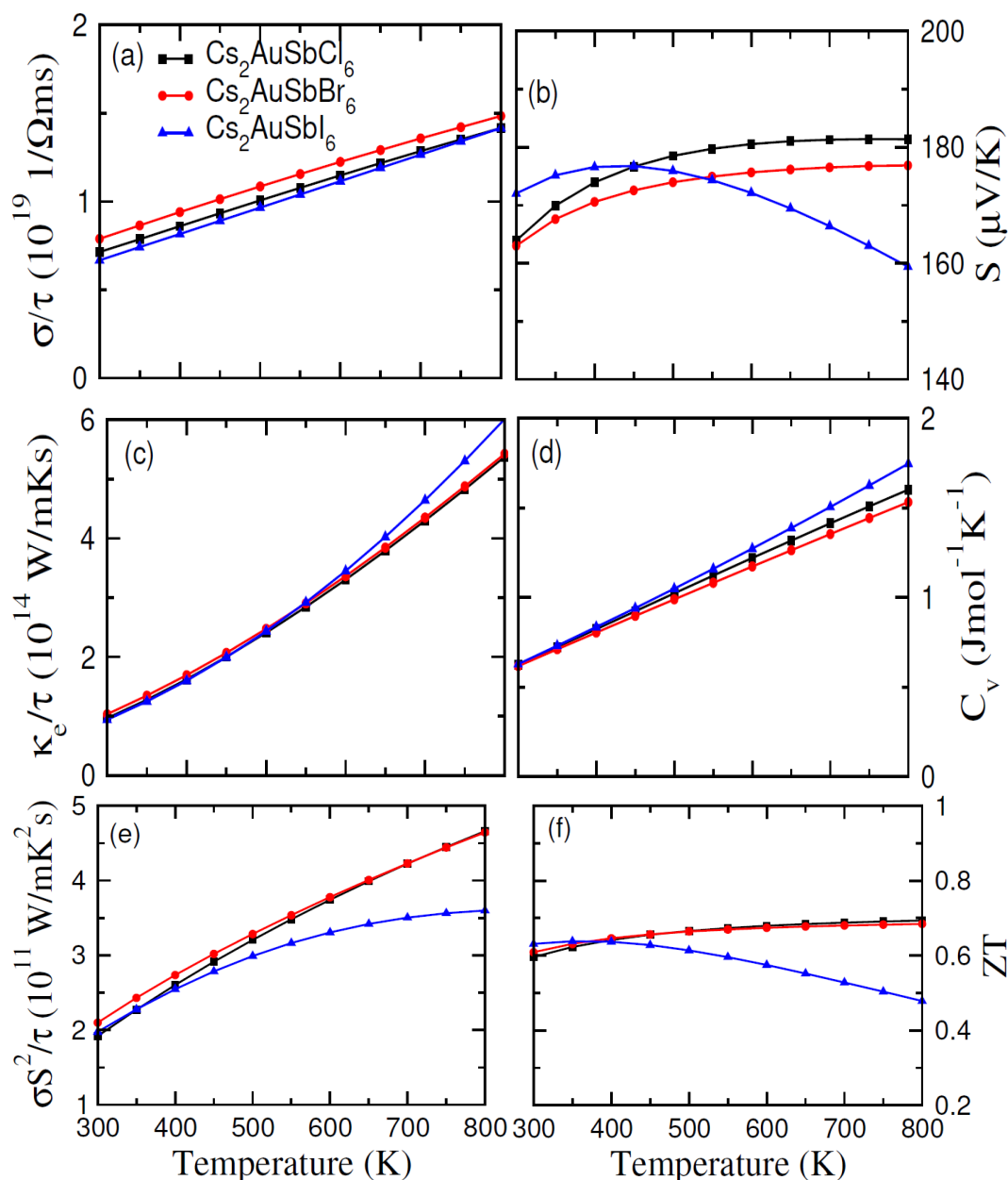


Fig. 7. The calculated (a) electrical conductivity (σ/τ), (b) Seebeck coefficients (S), (c) thermal conductivity (κ_e/τ), (d) Specific heat capacity (C_v), (e) power factor and figure of merit (ZT) against temperature and chemical potential of HDPs $\text{Cs}_2\text{AuSbX}_6$ ($X = \text{Cl}, \text{Br}, \text{I}$).

4. Conclusion

In summary, $\text{Cs}_2\text{AuSbX}_6$ ($X = \text{Cl}, \text{Br}, \text{I}$) Pb-free double perovskites were the subject of our analytical investigation, which focused on the crystalline structure, mechanical characteristics, optoelectronic attributes, DOS, along with thermoelectric features of these materials. Following the optimization of the structure by the use of the PBEsol-GGA estimation, the energy level of the ground state was determined, and the lattice parameters were optimized. This was done before the determination of the properties. By calculating the formation enthalpy, we were able to ascertain whether or not the production of certain combinations was thermodynamically acceptable. The fact that all three combinations had negative values of -2.31 eV, -2.03 eV, and -1.89 for the enthalpy of formation ensured that the formation of either compound was thermally favorable.

As a result of the inclusion of Br and I at the Cl site, the fundamental structure parameter raised from 10.75 to 11.27 and 12.01Å, while the bulk modulus fell from 31.01 to 26.27 and 21.68GPa respectively. In the course of the research, the malleable and anisotropy nature of the components under investigation was verified by the application of moduli of elasticity calculations that are dependent on the constants of elasticity. On the flip side, when halide size increased, the stable values of the refractive index, reflectivity, and dielectric factor all rose. As the temperature increased, the values of electrical conductivity, heat conductivity, Seebeck's coefficient, power ratio, and figure of merit increased as well. Additionally, the replacement of Br and I at the Cl site ensured that these compounds were suitable for use in contemporary power generation systems.

Funding

Researchers Supporting Project number (RSPD2024R952), King Saud University

Acknowledgements

The authors extend their deep appreciation to Researchers Supporting Project number (RSPD2024R952), King Saud University, Riyadh, Saudi Arabia.

References

- [1] Nabi, M., Gupta, D. C. (2021), Scientific reports, 11(1), 1-13; <https://doi.org/10.1038/s41598-021-92443-1>
- [2] Ali, M. A., Dar, S. A., AlObaid, A. A., Al-Muhimeed, T. I., Hegazy, H. H., Nazir, G., Murtaza, G. (2021), Journal of Physics and Chemistry of Solids, 159, 110258; <https://doi.org/10.1016/j.jpcs.2021.110258>
- [3] Husin, H., Zaki, M. (2021), Protection and Control of Modern Power Systems, 6(1), 1-18; <https://doi.org/10.1186/s41601-021-00181-3>
- [4] Zhao, H., Liu, G., You, S., Camargo, F. V., Zavelani-Rossi, M., Wang, X., Gong, X. (2021), Energy & Environmental Science, 14(1), 396-406; <https://doi.org/10.1039/D0EE02235G>
- [5] Mitrašinović, A. M. (2021), Energy, 237, 121510; <https://doi.org/10.1016/j.energy.2021.121510>
- [6] Chu, Y., Meisen, P. (2011), Review and comparison of different solar energy technologies, Global Energy Network Institute (GENI), San Diego, CA, 1, 1-52.
- [7] Metayer, M., Breyer, C., Fell, H. J. (2015, September), 31st European Photovoltaic Solar Energy Conference and Exhibition (Vol. 5).
- [8] Kalair, A., Abas, N., Saleem, M. S., Kalair, A. R., Khan, N. (2021), Energy Storage, 3(1), e135; <https://doi.org/10.1002/est2.135>
- [9] Ringsmuth, A. K., Landsberg, M. J., Hankamer, B. (2016), Renewable and Sustainable Energy Reviews, 62, 134-163; <https://doi.org/10.1016/j.rser.2016.04.016>
- [10] Jha, A. R. (2009), Solar cell technology and applications, Auerbach publications; <https://doi.org/10.1201/9781420081787>
- [11] Singh, B. P., Goyal, S. K., Kumar, P. (2021), Materials Today: Proceedings, 43, 2843-2849; <https://doi.org/10.1016/j.matpr.2021.01.003>
- [12] Isabela, C. B., Lameirinhas, R. A. M., Torres, J. P. N., Fernandes, C. A. (2021), Sustainable Energy & Fuels, 5(8), 2273-2283; <https://doi.org/10.1039/D0SE01717E>
- [13] Cao, J., Yan, F. (2021). Energy & Environmental Science, 14(3), 1286-1325; <https://doi.org/10.1039/D0EE04007J>

- [14] Jeong, J., Kim, M., Seo, J., Lu, H., Ahlawat, P., Mishra, A., Yang, Y., Hope, M.A., Eickemeyer, F.T., Kim, M. Yoon, Y.J., 2021, *Nature*, 592 (7854) 381-385; <https://doi.org/10.1038/s41586-021-03406-5>
- [15] Liu, D., Li, Q., Hu, J., Jing, H., & Wu, K. (2019), *Journal of Materials Chemistry C*, 7(2), 371-379; <https://doi.org/10.1039/C8TC04065F>
- [16] Li, B., Zhang, Y., Fu, L., Yu, T., Zhou, S., Zhang, L., Yin, L. (2018), *Nature communications*, 9(1), 1-8; <https://doi.org/10.1038/s41467-018-03169-0>
- [17] Schileo, G., Grancini, G. (2021), *Journal of Materials Chemistry C*, 9(1), 67-76; <https://doi.org/10.1039/D0TC04552G>
- [18] Liu, C., Li, W., Fan, J., Mai, Y. (2018), *Journal of energy chemistry*, 27(4), 1054-1066; <https://doi.org/10.1016/j.jechem.2017.10.028>
- [19] Kung, P. K., Li, M. H., Lin, P. Y., Jhang, J. Y., Pantaler, M., Lupascu, D. C., Chen, P. (2020), *Solar RRL*, 4(2), 1900306; <https://doi.org/10.1002/solr.201900306>
- [20] Du, K. Z., Meng, W., Wang, X., Yan, Y., Mitzi, D. B. (2017), *Angewandte Chemie International Edition*, 56(28), 8158-8162; <https://doi.org/10.1002/anie.201703970>
- [21] Pazoki, M., Jacobsson, T. J., Hagfeldt, A., Boschloo, G., Edvinsson, T. (2016), *Physical Review B*, 93(14), 144105; <https://doi.org/10.1103/PhysRevB.93.144105>
- [22] Murugan, P., Hu, T., Hu, X., Chen, Y. (2021), *Advanced Optical Materials*, 9(17), 2100390; <https://doi.org/10.1002/adom.202100390>
- [23] Roy, P., Sinha, N. K., Tiwari, S., Khare, A. (2020), *Solar Energy*, 198, 665-688; <https://doi.org/10.1016/j.solener.2020.01.080>
- [24] Keshavarz, M., Debroye, E., Ottesen, M., Martin, C., Zhang, H., Fron, E., Hofkens, J. (2020), *Advanced Materials*, 32(40), 2001878; <https://doi.org/10.1002/adma.202001878>
- [25] Blaha, P., Schwarz, K., Madsen, G. K., Kvasnicka, D., Luitz, J. (2001), *wien2k. An augmented plane wave+ local orbitals program for calculating crystal properties*, 60.
- [26] Ernzerhof, M., Perdew, J. P. (1998), *The Journal of Chemical Physics*, 109(9), 3313-3320; <https://doi.org/10.1063/1.476928>
- [27] Traoré, B., Boudier, G., Lafargue-Dit-Hauret, W., Rocquefelte, X., Katan, C., Tran, F., Kepenekian, M. (2019), *Physical Review B*, 99(3), 035139; <https://doi.org/10.1103/PhysRevB.99.035139>
- [28] Madsen, G. K., Singh, D. J. (2006), *Computer Physics Communications*, 175(1), 67-71; <https://doi.org/10.1016/j.cpc.2006.03.007>
- [29] Winiarski, M. J., Koziel, K., Sadecka, K., Dereń, P. J. (2020), *Solid State Communications*, 314, 113936; <https://doi.org/10.1016/j.ssc.2020.113936>
- [30] A. Jain, S. P. Ong, G. Hautier, W. Chen, W. D. Richards, S. Dacek, S. Cholia, D. Gunter, D. Skinner, G. Ceder, K. A. Persson, *APL Materials*, 1 (2013), 011002; <https://doi.org/10.1063/1.4812323>
- [31] Iqbal, S., Mustafa, G. M., Asghar, M., Noor, N. A., Iqbal, M. W., Mahmood, A., Shin, Y. H. (2022), *Materials Science in Semiconductor Processing*, 143, 106551; <https://doi.org/10.1016/j.mssp.2022.106551>
- [32] Flemban, T. H., Zelai, T., Mahmood, Q., Devi, A. A. S., Sajjad, M., Alhossainy, M. H., Amin, M. A. (2022), *Journal of Alloys and Compounds*, 894, 162313; <https://doi.org/10.1016/j.jallcom.2021.162313>
- [33] Fedorovskiy, A. E., Drigo, N. A., Nazeeruddin, M. K. (2020), *Small Methods*, 4(5), 1900426; <https://doi.org/10.1002/smt.201900426>
- [34] Bartel, C. J., Sutton, C., Goldsmith, B. R., Ouyang, R., Musgrave, C. B., Ghiringhelli, L. M., Scheffler, M. (2019), *Science advances*, 5(2), eaav0693; <https://doi.org/10.1126/sciadv.aav0693>
- [35] Faghinasiri, M., Beheshtian, J., Shayeganfar, F., Shahsavari, R. (2020), *Physical Chemistry Chemical Physics*, 22(10), 5959-5968; <https://doi.org/10.1039/C9CP05342E>
- [36] Jia, X., Zhang, H. Q., Wang, Z., Jiang, C. L., Liu, Q. J., Liu, Z. T. (2017), *Moscow University Physics Bulletin*, 72(4), 358-363; <https://doi.org/10.3103/S0027134917040154>

- [37] Mahmood, Q., Ghrib, T., Rached, A., Laref, A., Kamran, M. A. (2020), *Materials Science in Semiconductor Processing*, 112, 105009; <https://doi.org/10.1016/j.mssp.2020.105009>
- [38] Menedjhi, A., Bouarissa, N., Saib, S., Boucenna, M., Mezrag, F. (2020), *Acta Physica Polonica A*, 137(4), 486; <https://doi.org/10.12693/APhysPolA.137.486>
- [39] Connor, B. A., Biega, R. I., Leppert, L., Karunadasa, H. I. (2020), *Chemical science*, 11(29), 7708-7715; <https://doi.org/10.1039/D0SC01580F>
- [40] Szotek, Z., Temmerman, W. M., Svane, A., Petit, L., Winter, H. (2003), *Physical Review B*, 68(10), 104411; <https://doi.org/10.1103/PhysRevB.68.104411>
- [41] Kobayashi, M., Tanaka, K., Fujimori, A., Ray, S., Sarma, D. D. (2007), *Physical review letters*, 98(24), 246401; <https://doi.org/10.1103/PhysRevLett.98.246401>
- [42] Rai, D. P., Shankar, A., Ghimire, M. P., Thapa, R. K. (2015), *Computational Materials Science*, 101, 313-320; <https://doi.org/10.1016/j.commatsci.2015.01.027>
- [43] Yang, B., Mao, X., Hong, F., Meng, W., Tang, Y., Xia, X., Han, K. (2018), *Journal of the American Chemical Society*, 140(49), 17001-17006; <https://doi.org/10.1021/jacs.8b07424>
- [44] R. Varadwaj, P. (2020), *Nanomaterials*, 10(5), 973; <https://doi.org/10.3390/nano10050973>
- [45] Penn, D.R., 1962, *Physical Review* 128(5), 2093; <https://doi.org/10.1103/PhysRev.128.2093>
- [46] Chanda, S., Saha, S., Dutta, A., Sinha, T. P. (2015), *Materials Research Bulletin*, 62, 153-160; <https://doi.org/10.1016/j.materresbull.2014.11.021>
- [47] Ray, A., Basu, T., Behera, B., Gavali, D. S., Thapa, R., Vajandar, S., Nayak, P. (2020), *Materials Chemistry and Physics*, 239, 122250; <https://doi.org/10.1016/j.matchemphys.2019.122250>
- [48] Rai, D. P., Shankar, A., Ghimire, M. P., Thapa, R. K. (2015), *Computational Materials Science*, 101, 313-320; <https://doi.org/10.1016/j.commatsci.2015.01.027>
- [49] Al-Qaisi, S., Rai, D. P., Haq, B. U., Ahmed, R., Vu, T. V., Khuili, M., Alhashim, H. H. (2021), *Materials Chemistry and Physics*, 258, 123945; <https://doi.org/10.1016/j.matchemphys.2020.123945>
- [50] Mukhtar, M. W., Ramzan, M., Rashid, M., Naz, G., Imran, M., Fahim, F., Mahmood, Q. (2021), *Materials Science and Engineering: B*, 273, 115420; <https://doi.org/10.1016/j.mseb.2021.115420>
- [51] Ryu, B., Chung, J., Park, S. (2021), *Iscience*, 24(9), 102934; <https://doi.org/10.1016/j.isci.2021.102934>
- [52] Kumar, A., Bano, S., Govind, B., Bhardwaj, A., Bhatt, K., Misra, D. K. (2021), *Journal of Electronic Materials*, 50(11), 6037-6059; <https://doi.org/10.1007/s11664-021-09153-7>
- [53] Jeong, H., Kihoi, S. K., Kim, H., Lee, H. S. (2021), *Journal of Materials Research and Technology*, 15, 6312-6318; <https://doi.org/10.1016/j.jmrt.2021.11.065>
- [54] Lee, K. H., Kim, S. I., Lim, J. C., Cho, J. Y., Yang, H., Kim, H. S. (2022), *Advanced Functional Materials*, 2203852; <https://doi.org/10.1002/adfm.202203852>
- [55] Nasani, N., Kovalevsky, A. V., Xie, W., Rasekh, S., Constantinescu, G., Weidenkaff, A., Fagg, D. P. (2020), *The Journal of Physical Chemistry C*, 124(24), 13017-13025; <https://doi.org/10.1021/acs.jpcc.0c03149>
- [56] Xu, T., Haruna, A. Y., Ma, Z., Li, W., Li, J., Luo, Y., Yang, J. (2021). *Chemistry of Materials*, 33(20), 8097-8105; <https://doi.org/10.1021/acs.chemmater.1c02895>
- [57] Alam, H., Ramakrishna, S. (2013), *Nano energy*, 2(2), 190-212; <https://doi.org/10.1016/j.nanoen.2012.10.005>
- [58] Alam, H., Ramakrishna, S. (2013), *Nano energy*, 2(2), 190-212. <https://doi.org/10.1016/j.nanoen.2012.10.005>